Eur. Phys. J. B **23**, 463–472 (2001)

THE EUROPEAN PHYSICAL JOURNAL B

EDP Sciences
© Società Italiana di Fisica
Springer-Verlag 2001

The spin-crossover complex [Fe(tpa)(NCS)$_2$]

Investigated by synchrotron-radiation based spectroscopies

H. Paulsen[1,a], H. Grünsteudel[2,4], W. Meyer-Klaucke[3], M. Gerdan[1], H.F. Grünsteudel[4], A.I. Chumakov[4], R. Rüffer[4], H. Winkler[1], H. Toftlund[2], and A.X. Trautwein[1]

[1] Institut für Physik, Medizinische Universität Lübeck, Ratzeburger Allee 160, 23538 Lübeck, Germany
[2] Department of Chemistry, University of Southern Denmark, Odense Campus, 5230 Odense, Denmark
[3] EMBL Outstation Hamburg, Notkestr. 85, 22603 Hamburg, Germany
[4] European Synchrotron Radiation Facility, BP 220, 38043 Grenoble, France

Received 19 June 2001

Abstract. The temperature-induced spin crossover of iron(II) in the [Fe(tpa)(NCS)$_2$] complex has been investigated by nuclear forward scattering (NFS), nuclear inelastic scattering (NIS), extended X-ray absorption fine structure (EXAFS) spectroscopy, conventional Mössbauer spectroscopy (MS) and by measurements of the magnetic susceptibility (SQUID). The various measurements consistently show that the transition is complete and abrupt and exhibits a hysteresis between 102 and 110 K. The dependence of the hyperfine parameters of the high-spin (HS) and of the low-spin (LS) phase on temperature is gradual while the effective thickness (determined by the Lamb-Mössbauer factor f_{LM}) shows a step at the transition temperature. This step could be identified clearly because the effective thickness is measured directly by NFS. The Lamb-Mössbauer factor, the Debye temperature and the mean-square displacement of iron(II) could be determined for the HS and for the LS phase. When comparing the NIS data with the results from density functional theory (DFT), the Fe-N stretching vibrations of both LS and HS phases could be unambiguously identified and the f_{LM} could be factorized for both phases into a lattice and a molecular part. The structural information from EXAFS and DFT geometry optimization are in reasonable agreement.

PACS. 33.25.+k Nuclear resonance and relaxation – 76.80.+y Mössbauer effect; other gamma-ray spectroscopy – 31.15.Ew Density-functional theory

1 Introduction

The iron(II) complex [Fe(tpa)(NCS)$_2$] (tpa = tris(2-pyridylmethyl)amine) (Fig. 1) belongs to the family of thermally driven spin-crossover complexes, which exhibit a transition from a low-spin (LS) to a high-spin (HS) state by increasing the temperature. These complexes are promising materials for optical information storage and display devices [1]. The thermally driven LS $\rightleftharpoons$ HS conversion of octahedral iron(II) complexes has been well studied in the past and is summarized in several review articles, *e.g.* [1,2]. The large family of spin-crossover complexes can be divided in groups which show either a gradual or an abrupt transition with and without hysteresis when decreasing and increasing the temperature. A detailed investigation of the condition for the thermally induced spin crossover to take place allows an insight into the fundamental mechanisms governing metal coordination chemistry. The knowledge of the Lamb-Mössbauer

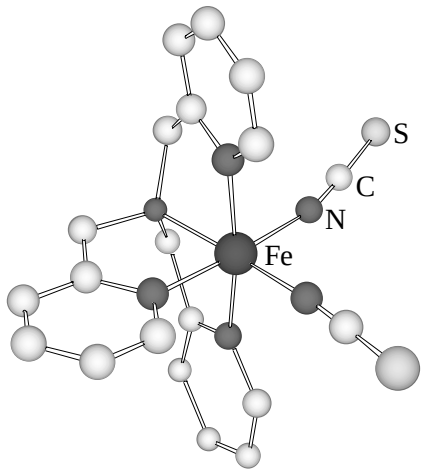

Fig. 1. Geometry of the LS isomer of [Fe(tpa)(NCS)$_2$] calculated with DFT. Hydrogen atoms are not shown for clarity.

[a] e-mail: paulsen@physik.mu-luebeck.de

factor f_{LM} provides information on the dynamics of such systems as already demonstrated by Jung *et al.* [3,4]. The precise determination of f_{LM} *via* conventional Mössbauer spectroscopy (MS) is difficult, because a number of parameters like the background of nonresonant radiation and the f_{LM}-factor of the source have to be known accurately. Therefore the novel method of nuclear forward scattering (NFS) was used to determine the effective thickness directly from the measured data and to complement previous studies. Furtheron also nuclear inelastic scattering (NIS) has been applied for the HS and the LS phase in order to measure the iron partial phonon density of states of each phase and to compare these with calculations of the molecular vibrations applying density functional theory (DFT). The iron-ligand distances derived from DFT geometry optimizations have been compared with results obtained from the extended X-ray absorption fine structure (EXAFS) of the complex. The spin transition behavior has been checked with susceptibility measurements and the hyperfine parameters of both phases have been documented by NFS and by conventional MS. For all measurements polycrystalline $[\mathrm{Fe(tpa)(NCS)_2}]$ with an enrichment in ^{57}Fe of 20% was used.

1.1 Nuclear resonant scattering

When a synchrotron radiation pulse ($\approx$ 100 ps long) penetrates a sample containing resonant nuclei like ^{57}Fe, electronic X-ray scattering happens instantaneously ($t = 0$) while processes involving nuclear excitations are delayed (the excited nuclear state of ^{57}Fe has a mean life time $\tau_0 = 141$ ns). Therefore it is possible to separate the events originating from nuclear and electronic scattering in the sample. In general a nuclear scattering process can proceed coherently or incoherently.

In the coherent case the incident 14.4 keV photons are scattered by the ensemble of resonant nuclei in the sample. Due to interference effects the scattered radiation originating from different nuclei is forward directed [5], and the hyperfine structure of the nuclear transition leads to quantum beats, *i.e.* to a modulation of the intensity of this forward scattered radiation. Taking two nuclear hyperfine transitions with energy difference $\hbar\Delta\omega = \hbar(\omega_{02} - \omega_{01})$ and assuming equal weight of the transitions, as it is the case for the pure LS and HS phases in the present study, the forward scattered intensity for an infinitely thin sample can be written as [6]

$$I_{\mathrm{fwd}}(t) \sim \mathrm{e}^{-\tau}\left[1 + \cos(\Delta\omega t)\right], \tag{1}$$

where $\tau = t/\tau_0$ is time in units of the nuclear lifetime. From the beat structure the hyperfine splitting of the excited and ground nuclear states and the energy shifts due to different chemical or magnetic environment of the different nuclear sites can be derived. With the zero positions in equation (1) the splitting ΔE_{hf} can be estimated *via* the measured quantum beat period T:

$$\Delta E_{\mathrm{hf}} \approx h/T. \tag{2}$$

Another important feature of coherent scattering by a large ensemble of nuclei is the speed-up of the nuclear decay and the modulation of the time evolution due to multiple scattering. The general expression for the measured NFS intensity for a single transition in a sample with finite thickness d is [5,6]

$$I_{\mathrm{fwd}}(t) \sim \frac{\Gamma_0}{\Delta E_\gamma}\frac{t_{\mathrm{eff}}}{4\tau\tau_0}\mathrm{e}^{-\tau-\sigma_{\mathrm{el}}nd}\left[J_1\left(\sqrt{t_{\mathrm{eff}}\tau}\right)\right]^2. \tag{3}$$

$\Gamma_0 = \hbar/\tau_0$ denotes the natural linewidth for the nuclear transition in ^{57}Fe, ΔE_γ is the bandwidth of the monochromator system, σ_{el} is the electronic part of the cross section per atom, n is the density of resonant nuclei in the target, J_1 is the Bessel function of first order and t_{eff} the effective thickness of the target:

$$t_{\mathrm{eff}} = d\, n\, f_{\mathrm{LM}}\, \sigma_0, \tag{4}$$

where σ_0 denotes the maximum resonance cross section which is the nuclear part of the absorption cross section per atom at nuclear resonance energy. The resulting time dependence of the intensity is an exponential decay modulated by the Bessel function. These dynamical beats, in contrast to quantum beats, do not have constant frequency, but the distance of the beats increases with time. The minima of the dynamical beats can be used to determine directly the effective thickness of the transition line and *via* equation (4) the Lamb-Mössbauer factor [7].

In the incoherent case [8] the scattering process is localized at a single nucleus due to various reasons:

(i) A single excited ^{57}Fe nucleus decays with 91.8% probability by nuclear internal conversion giving rise to fluorescence radiation with characteristic energies (mainly 6.4 keV in the case of iron).

(ii) Despite detuning the energy E_i of the incident synchrotron beam (which has an energy resolution of some meV) by $\gtrsim$ 10 meV nuclear resonance absorption is still possible if the energy difference between E_{i} and the nuclear resonance energy E_0 matches the energy E of a phonon in the sample, $E = E_i - E_0$, which, depending on whether $E_i > E_0$ or $E_i < E_0$, causes creation or annihilation of phonons.

(iii) Time-dependent hyperfine interactions (relaxation) cause changes of the nuclear states within the mean life time of the excited nuclear state.

Also in the incoherent scattering process the emitted radiation is delayed because in all cases, (i–iii), the nuclei are involved in the scattering process; however, it is no longer forward directed. Incoherent scattering includes scattering processes which are inelastic with respect to the vibrational state of the crystal. Therefore this scattering is termed also nuclear inelastic scattering (NIS). In NIS the isotropically scattered radiation is measured as a function of E. The resulting NIS spectrum $S(E)$ can be expressed as the sum of an elastic or zero-phonon contribution and of single- and multi-phonon terms (using the harmonic approximation and assuming for simplicity a cubic Bravais

lattice) [8,9]

$$S(E) = \underbrace{f_{\mathrm{LM}}\,\delta(E)}_{0\text{-phononpart}} + \underbrace{f_{\mathrm{LM}} \sum_{n=1}^{\infty} S_n(E)}_{n\text{-phononpart}}, \tag{5}$$

$$S_1(E) = \frac{E_{\mathrm{R}}}{E}\,\frac{g_{\mathrm{Fe}}(E)}{1-\mathrm{e}^{-\beta E}}\,,$$

$$S_n(E) = \frac{1}{n}\int_{-\infty}^{+\infty} S_1(E')\,S_{n-1}(E-E')\,\mathrm{d}E'.$$

$E_R = \hbar^2\mathbf{k}^2/2m_{\mathrm{Fe}}$ denotes the recoil energy of a free iron atom, $\mathbf{k}$ is the wavevector of the incident X-rays, m_{Fe} is the mass of the iron nucleus and $g_{\mathrm{Fe}}(E)$ is the iron partial density of phonon states. Since the elastic or zero-phonon part of the spectrum represents a resonant scattering process without recoil it is equal to the Lamb-Mössbauer factor [9]:

$$f_{\mathrm{LM}} = \mathrm{e}^{-2W}, \tag{6}$$

$$2W = \int_0^{+\infty} \frac{E_{\mathrm{R}}}{E}\,g_{\mathrm{Fe}}(E)\,\coth(\beta E/2)\,\mathrm{d}E.$$

2 Experimental and computational details

The nuclear resonance scattering data were obtained at the Nuclear Resonance Beamline ID 18 [10] of the European Synchrotron Radiation Facility (ESRF) in Grenoble, France. The experimental setup was standard for nuclear resonance scattering as described elsewhere (see *e.g.* [11]). The NFS data were collected in hybrid-bunch mode and the NIS data in 16-bunch mode.

The NFS measurements were performed between 34 K and room temperature upwards and downwards. In order not to trap the HS state, cooling was performed slowly with 0.1 K per minute in the transition region (90–110 K) and with 1 K per minute for all other temperatures. One spectrum, however, was taken after rapid cooling in order to determine the parameters related to the trapped HS state at low temperature. The data collection time for a single NFS spectrum was between 30 minutes and 4 hours, depending on the temperature of the sample. The evaluation of the NFS spectra has been performed using the program CONUSS [12].

NIS data were recorded at various X-ray energies which are detuned by E from the nuclear resonance energy. All photons scattered into a specific solid angle ($\approx 2\pi$ sterad) were collected by integrating over the delay time which is given by the time interval between two bunches.

K-edge EXAFS data were collected in absorption mode at beam line D2 of the European Molecular Biology Laboratory, Outstation Hamburg, with a positron beam energy of 4.6 GeV and a maximum stored current of 100 mA. The synchrotron radiation beam was monochromatised using a Si(111) double crystal monochromator [13]. Harmonic rejection was achieved by detuning the monochromator to 50% of its peak intensity and by a focusing Au-coated mirror. The sample was located in a closed-cycle He cryostat. An energy resolution better than 2.0 eV was achieved.

Conventional Mössbauer spectra were obtained in absorption geometry. The ^{57}Co[Rh] source was driven with constant acceleration. The energy calibration was performed with α-iron at room temperature and the isomer shift is relative to this standard. Mössbauer spectra recorded at various temperatures were fitted with the transmission integral using CONUSS [12].

For the magnetic measurements a SQUID magnetometer of the type MPMS Quantum Design was used. The applied field was 1 T for all temperatures. The magnetic susceptibility measurements were performed at various temperatures between 2 K and 295 K by increasing and by decreasing the temperature. The effective magnetic moment μ_{eff} expressed in units of the Bohr magneton μ_{B} was derived from the experimental data by

$$\mu_{\mathrm{eff}} = \mu_{\mathrm{B}}\sqrt{8T(w_{\mathrm{mol}}\chi_{\mathrm{mass}} - \chi_D)}\,. \tag{7}$$

In this expression $\chi_D = -220\times10^{-6}$ cm^3 mol^{-1} denotes the molar diamagnetic susceptibility which was estimated from Pascals constants [14], $w_{\mathrm{mol}} = 471.453$ g mol^{-1} is the molecular weight of [Fe(tpa)(NCS)$_2$] and χ_{mass} the experimental mass susceptibility at temperature T.

For the HS and the LS isomers of [Fe(tpa)(NCS)$_2$] electronic structure calculations were performed using the DFT method B3LYP [15] implemented in the GAUSSIAN98 program system [16] together with the split valence 6-311G* basis set for H, C, N and S and the Wachters-Hay double zeta basis for Fe [17]. The geometries were fully optimized and the normal modes of molecular vibration were calculated within the harmonic approximation for the optimized geometries. The resulting vibrational frequencies were corrected by the scaling factor 0.9613 as has been proposed by Wong [18] for the 6-31G* basis set. The calculated normal modes for both isomers have been used to simulate the absorption probability density $S(E)$, equation (5), according to the procedure described elsewhere [19].

3 Results and discussion

3.1 SQUID and MS measurements

Above the spin transition, at 295 K, the measured effective magnetic moment $\mu_{\mathrm{eff}} = 5.35\mu_{\mathrm{B}}$ is larger than expected from the "spin-only" value $\mu_{\mathrm{so}} \approx 4.9\mu_{\mathrm{B}}$ for $S = 2$ of a ferrous high-spin complex. The same behavior was earlier reported for similar compounds and was attributed in addition to the spin, to orbital contributions [20]. In the LS phase $\mu_{\mathrm{eff}} = 1.1\mu_{\mathrm{B}}$ was measured. The deviation of the effective magnetic moment for the LS phase from zero is due to an incomplete transition as shown by the MS data (Tab. 1). For better comparison of the measured data with those of the other methods the revealed effective magnetic moment is expressed as fraction of HS as shown in Figure 2. The transition occurs abrupt and exhibits a narrow hysteresis of about 5 K around 106 K.

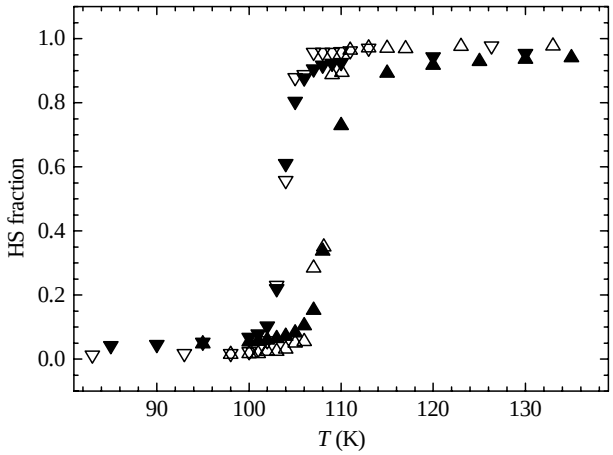

Fig. 2. HS fraction in the region of the transition temperature measured by SQUID (solid triangles) and NFS (open triangles). The values derived during a temperature scan with increasing (decreasing) temperature are marked with up triangles (down triangles). The NFS data are shifted by 3 K to higher temperature.

Table 1. Parameters for $[Fe(tpa)(NCS)_2]$ obtained from conventional MS. HS_2 denotes the second HS state which can be neglected for higher temperatures but which has to be taken into account for low temperatures in order to obtain a reasonable fit.

T (K)		Fraction (%)	ΔE_Q ($mm\,s^{-1}$)	δ ($mm\,s^{-1}$)
	LS	98.0 ± 1.0	0.41 ± 0.01	0.49 ± 0.01
4.2 ± 0.1	HS	1.0 ± 0.5	2.46 ± 0.15	1.11 ± 0.15
	HS_2	1.0 ± 0.5	3.00 ± 0.15	1.11 ± 0.15
	LS	99.0 ± 1.0	0.40 ± 0.01	0.47 ± 0.01
77 ± 0.5	HS	0.5 ± 0.5	2.75 ± 0.15	1.11 ± 0.15
	HS_2	0.5 ± 0.5	2.80 ± 0.15	1.11 ± 0.15
	LS	4.0 ± 0.5	0.34 ± 0.15	0.47 ± 0.15
130 ± 0.5	HS	95.5 ± 1.0	2.51 ± 0.01	1.09 ± 0.01
	HS_2	0.5 ± 0.5	2.60 ± 0.15	1.09 ± 0.15
	LS	1.0 ± 0.5	0.34 ± 0.15	0.52 ± 0.15
200 ± 0.5	HS	98.5 ± 1.0	2.32 ± 0.01	1.05 ± 0.01
	HS_2	0.5 ± 0.5	2.30 ± 0.15	1.05 ± 0.15

3.2 NFS measurements

A selection of the measured NFS spectra at various temperatures is shown in Figure 3. At 133 K the regular quantum beat structure reflects the quadrupole splitting from the pure HS phase. The envelope reflects the dynamical beating and shows a minimum around 200 ns. Below the transition, at 83 K, the quantum beats appear with lower frequency due to the smaller quadrupole splitting of the LS state. Here the minima of the quantum beats coincide with the dynamical beats, hence it is difficult to distinguish them by eye. The computer analysis of this spectrum reveals the quadrupole splitting and the Lamb-Mössbauer-factor of the LS isomer and also two additional HS phases, which are also seen in the conventional Mössbauer spectra and were also present in earlier measurements [21]. It turned out that in the whole temperature range a second HS phase is present, which, however, does not exhibit spin crossover. The fraction of this second HS phase is only about 1%. The analysis of the NFS spectra without this phase delivers at high temperatures a fit with approximately the same quality as the fit with this phase. At low temperatures the quality of the fits definitely improves by adding this phase.

The NFS measurements yield a temperature dependence of the fraction of molecules in the HS state which is in agreement with the data obtained from MS or SQUID measurements (see Fig. 2), provided that the NFS data are shifted by 3 K to higher temperatures. This correction is plausible, because during the MS and SQUID measurements the sample was surrounded by exchange gas whereas during the NFS measurements it was mounted on a cold finger in vacuum. Taking the temperature of the MS and SQUID data as absolute, the spin-crossover takes place within approximately 5 K at $T_{HS\rightarrow LS} = 103.7$ K (for decreasing temperature) and $T_{LS\rightarrow HS} = 108.8$ K (for increasing temperature).

The NFS and MS quadrupole splittings ΔE_Q of the diamagnetic LS isomer remain nearly constant over the whole temperature range whereas the NFS and MS quadrupole splittings of both HS phases decrease with increasing temperature, which is the typical behaviour for ferrous high-spin complexes [22]. The NFS values for the isomer shift δ reflect the relative shift of the HS phases against the LS phase. The two HS phases are not shifted with respect to each other. Neither ΔE_Q nor δ of LS and HS isomers change abruptly upon spin transition.

The temperature dependence of the effective thickness t_{eff} obtained from the NFS data is shown in Figure 4. t_{eff} is growing with decreasing temperature. The step in the transition region is pronounced: on the branch measured with decreasing temperature it changes from $t_{eff} = 26.5$ to 30.1 and with increasing temperature from $t_{eff} = 29.4$ to 25.4. This direct and accurate measure of the discontinous behavior of t_{eff} in the transition region confirms earlier, less accurate results obtained with MS from similar compounds [23,24].

According to equation (4) the Lamb-Mössbauer factor can be obtained from t_{eff} if the sample thickness and the density of resonant nuclei in the sample are known. The density of resonant nuclei was calculated from the density of the corresponding single crystalline compound (1.475 g/cm^3), the chemical composition of the complex ($C_{20}H_{18}N_6S_2Fe$) and the abundance of ^{57}Fe (20%). The thickness was determined applying two different methods: (i) From the size of the absorber holder and the weight of the sample the thickness was calculated to be 600 μm±20%. The large error is due to the geometry of the sample holder. (ii) *Via* electronic absorption the thickness of the sample was determined to be 705 $\mu m \pm 5\%$ over the whole sample area. The small error in the latter case was estimated from the inhomogeneity of the polycrystalline sample which was checked by scanning the synchrotron

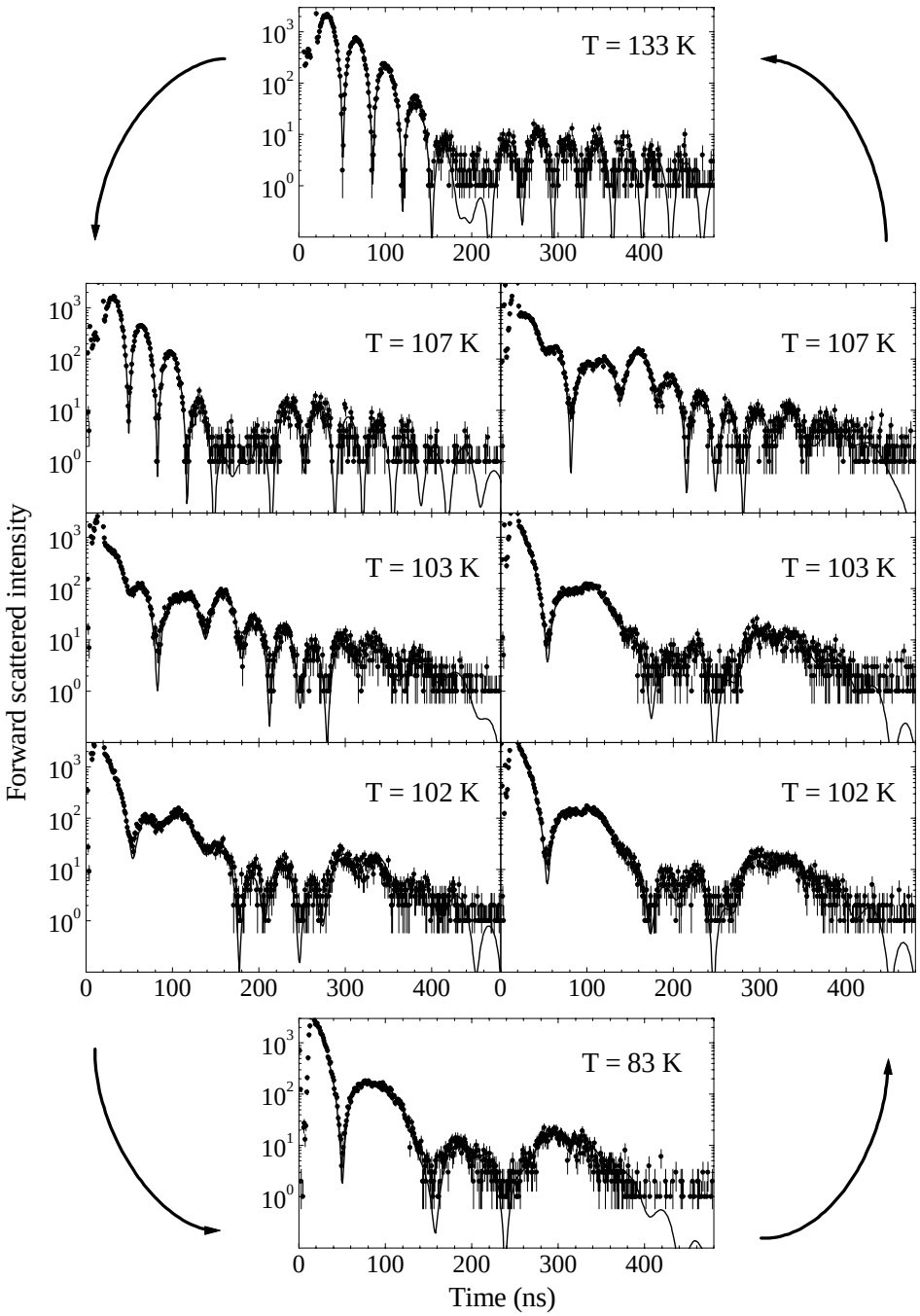

Fig. 3. Time evolution of the NFS intensity for various temperatures around the HS-LS transition. The measurements were performed at ID18, ESRF in hybrid-bunch mode. The left-hand side shows measurements in the transition region performed with decreasing temperature and the right-hand side with increasing temperature. The points give the measured data and the curves are results from calculations performed with CONUSS [12].

beam (2 mm × 0.2 mm) over the whole sample area. The two values obtained for the sample thickness agree within the error margins. For calculating f_{LM} of the HS and LS states the value 705 μm for the sample thickness was used. For the LS state f_{LM} is larger than that for the HS state (Fig. 5a), reflecting weaker iron-ligand bonds in the HS state compared to the LS state. This observation from NFS is confirmed by NIS and DFT results (vide infra, Tab. 3).

Using the harmonic approximation for cubic crystals and the Debye model, the Debye temperature Θ_{D} of the whole system can be derived from f_{LM} and from the temperature T of the sample [25]:

$$f_{\mathrm{LM}}(T) = \exp\left\{\frac{-3E_R}{2k_{\mathrm{B}}\Theta_{\mathrm{D}}}\left[1+\frac{4T}{\Theta_{\mathrm{D}}}\int_0^{\Theta_D/T}\frac{x}{\mathrm{e}^x-1}\mathrm{d}x\right]\right\}, \quad (8)$$

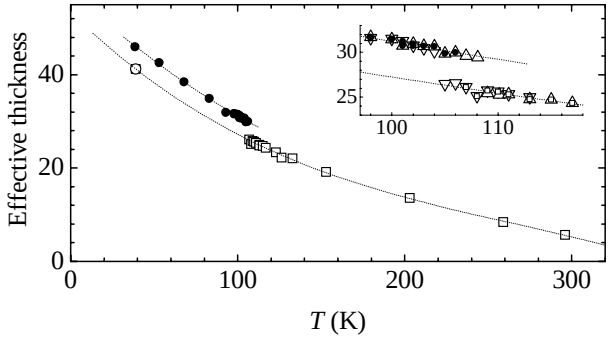

Fig. 4. Effective thickness derived from NFS measurements. The open squares (solid circles) denote measurements with a fraction of high-spin (low-spin) higher than 95%. The open circle denotes the trapped high-spin isomer obtained after rapid cooling. The insert shows the step in the transition region: The up triangles (down triangles) denote measurements recorded with decreasing (increasing) temperature. The lines are guides to the eyes.

were k_{B} stands for the Boltzmann constant. The Debye model represents only a very rough approximation of the phonon frequency spectrum. Corresponding to the behaviour of f_{LM} the Debye temperature Θ_{D} is larger for the LS state than for the HS state (Fig. 5b). Figure 5c shows the mean-square displacement (msd) of the iron nucleus in the molecule as derived from f_{LM}:

$$f_{\mathrm{LM}}(T) = \exp\left(-\langle x^2\rangle \mathbf{k}^2\right). \tag{9}$$

As a consequence of the general trend of the f_{LM} factors the obtained msd results show similar dependencies as previously obtained from another spin-transition complex using conventional MS [4], *i.e.* the iron atom in the HS state has a larger mean-square displacement than in the LS state.

In order to visualize the HS→LS transition in terms of NFS spectra a 3D plot of the NFS intensity was calculated for small temperature steps by interpolating the parameters obtained from the measured data (Fig. 6). The quantum beat structure abruptly changes at the transition temperature. Above the transition the beating is faster and more regular than below the transition. Also the temperature variation of the 1st minimum of the dynamical beats of the HS phase can be clearly seen (dashed line in Fig. 6). The corresponding 'valley' extends from about 800 ns at 300 K to 160 ns at the transition temperature. This behaviour represents an increase in the effective thickness t_{eff} from 5.2 to 26.5. Below the transition the 1st minimum of the dynamical beats of the LS phase can be hardly seen; the computer simulation shows that the corresponding 'valley' reaches 90 ns at 30 K which corresponds to $t_{\mathrm{eff}} \approx 47$.

3.3 NIS measurements

Nuclear inelastic scattering measurements with $[\mathrm{Fe(tpa)(NCS)_2}]$ were performed with two different

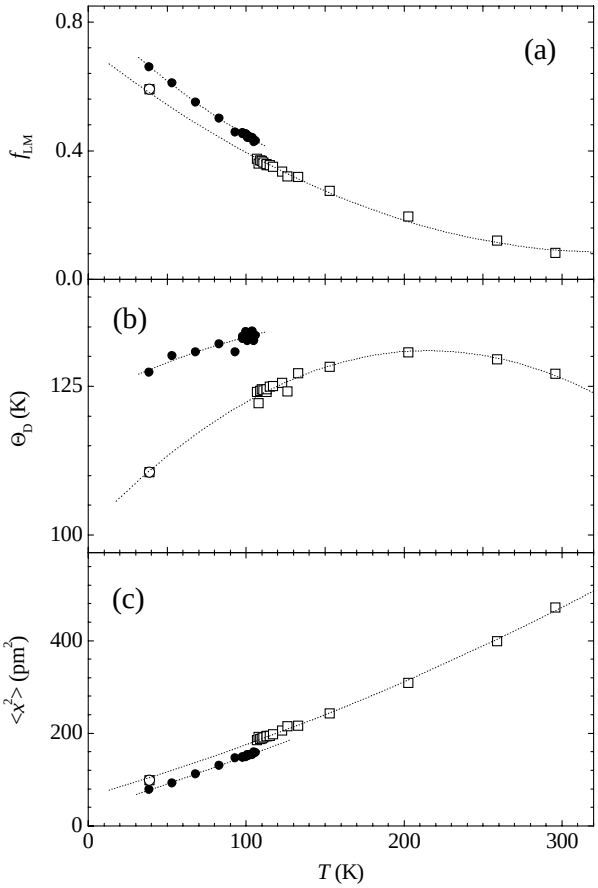

Fig. 5. Lamb-Mössbauer factor f_{LM} (a), Debye temperature Θ_{D} (b) and mean-square displacement $\langle x^2\rangle$ of the ^{57}Fe nucleus (c) derived from t_{eff}. In (a) values derived for a sample thickness of 705 μm are shown for the HS phase (open squares, >95% HS contribution) and for the LS phase (solid circles, >95% LS contribution). The open circles denote the frozen HS state (>95 % HS contribution). Note the step between values belonging to the HS and the LS state. The dotted lines are guides to the eyes.

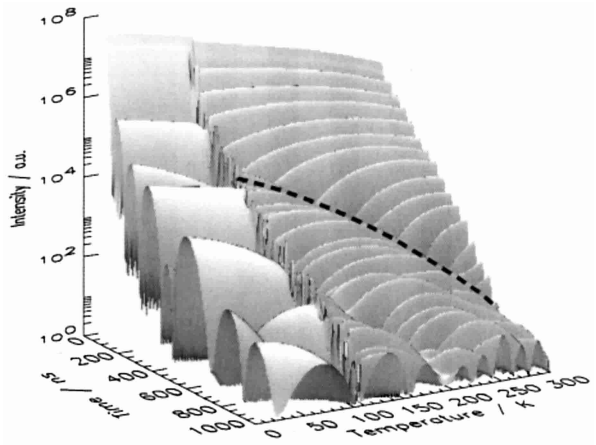

Fig. 6. 3D plot of the NFS intensity of $[\mathrm{Fe(tpa)(NCS)_2}]$. The spectra were calculated with CONUSS [12] using the parameters obtained from the NFS measurements. The dashed line indicates the variation of the 1st minimum of the dynamical beats of the HS phase with temperature.

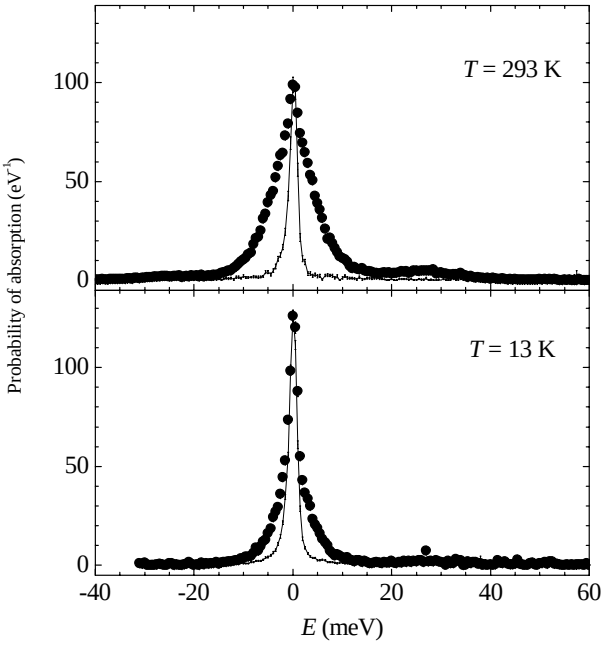

Fig. 7. NIS spectrum of [Fe(tpa)(NCS)$_2$] at different temperatures as indicated, measured with a HRM of 1.7 meV bandwidth. The solid circles represent the probability of absorption and the solid line the resolution function R(E) measured in forward direction and scaled to the maximum of the inelastic data.

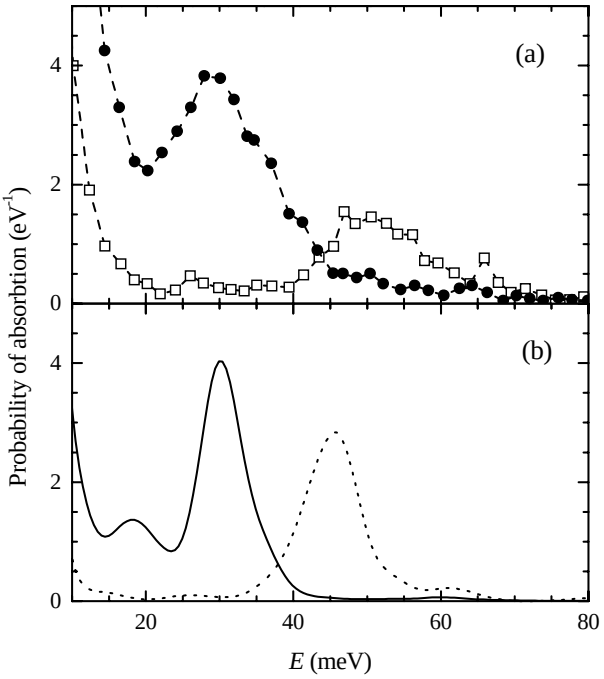

Fig. 8. (a) NIS spectra of the LS (solid circles) and HS (open squares) isomers of [Fe(tpa)(NCS)$_2$] measured with a HRM of 6.4 meV bandwidth. The dashed lines are guides to the eyes. The simulated NIS spectra (b) for the LS (dotted line) and for the HS isomer (solid line) were calculated with the B3LYP/6-311G* method.

sets of high resolution monochromators (HRM). The spectra were measured at ID18 with an energy resolution of $\Delta E_\gamma = 1.7$ meV in 2/3 filling mode and with $\Delta E_\gamma = 6.4$ meV in 16-bunch mode. The spin state of the complex was checked by recording simultaneously the NFS intensity in 16-bunch mode; in 2/3 filling mode this was not possible. The NIS spectra shown in Figures 7 and 8 are the sum of several individual energy scans as listed in Table 2. Contributions in the measured spectra with negative energy E account for annihilation and positive energy for creation of vibrations in the molecular complex. At low temperatures only low energy phonon states are occupied (2.5 meV corresponds to approximately 30 K), therefore annihilation of phonons is scarce in this temperature region. Creation of phonons, however, is possible at all vibrational energies of the complex under study. At elevated temperatures a symmetric broadening of the inelastic data around the resonance energy $E = 0$ (Fig. 7, upper panel) and a weak peak around 30 meV (HS phase, Fig. 8) is observed. At low temperatures the broadening of the central peak is slightly asymmetric (Fig. 7, lower panel) and the peak appears around 45 meV (LS phase, Fig. 8). The broadening around the central peak is much better resolved with the 1.7 meV HRM (than with the 6.4 meV HRM) but the peaks at higher energy vanish nearly in the noise level. The normalization of the measured data was performed making use of Lipkin's sum rules as described in [11,19].

IR measurements on several spin-crossover complexes with a central [FeN$_6$] octahedron indicate a remarkable increase of the Fe-N bond stretching frequencies from about 25 to 30 meV in the HS state to about 50 to 60 meV in the LS state. For the complex studied here Fe-N bond stretching frequencies of 59.5 and 66.0 meV were reported for the LS isomer [26]. NIS is a valuable alternative to IR and Raman spectroscopy; it easily extends below 35 meV, which is difficult to reach by IR, and, in addition, the Fe-N stretching modes can be definitely identified in the NIS spectra, whereas the IR and Raman spectra are rather complex in this energy region [27] making an unambiguous assignment of these modes very difficult.

The measured NIS spectra of the HS and LS isomers of [Fe(tpa)(NCS)$_2$] exhibit inelastic peaks of 12 and 7 meV linewidth, respectively, and an inelastic peak at 30 meV in the HS state and at 50 meV in the LS state

Table 2. Parameters for the NIS scans. ΔE_γ is the energy resolution of the monochromator, T is the temperature of the sample, t_m is the measuring time per energy point, n_s the number of scans added up and n_p the total number of points measured.

ΔE_γ (meV)	T (K)	t_m (s)	n_s	n_p
6.4	200	20	3	630
6.4	107	20	3	630
6.4	34	20	4	450
1.7	293	1	12	2600
1.7	14	1	31	4000
1.7	13	1	22	3200

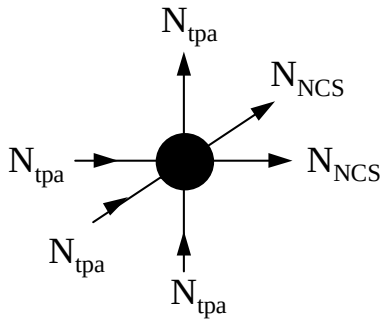

Fig. 9. A Fe-N bond stretching mode which can be observed by NIS requires a non-zero mean-square displacement of the iron atom.

(Fig. 8a) [11,19,28]. Comparing the intensity of the inelastic peaks in the HS and the LS spectrum it should be kept in mind, that the HS peak at 30 meV is located on the shoulder of the central peak. The LS spectrum exhibits another, rather small peak at 66 meV, which is not seen in the HS spectrum.

The linewidth ($\sim$12−15 meV) of the inelastic peaks observed at 30 meV (HS) and at 50 meV (LS) is by far broader than the resolution of the HRM (6.4 meV) and the linewidth of the central peak (7.2 meV). Assuming that these peaks are attributed to only one individual molecular vibration, the observed broadening might be caused either (i) by strong dispersion of the optical phonon branch that corresponds to this molecular mode, or (ii) by damping of this mode (*i.e.* dissipation of the energy of this mode into other vibrational modes due to anharmonicity) which leads to a very short lifetime of this mode (<1 ps). Neither of the two explanations can be strictly ruled out in the case of [Fe(tpa)$(NCS)_2$]. However, experimental data for similar spin-crossover complexes ([Fe(tptMetame)]$(ClO_4)_2$ [29] and [Fe$(bpp)_2$] [30]) do not exhibit such a broadening. NIS measurements for [Fe$(bpp)_2$] at different temperatures reveal that the linewidth of the observed peaks is roughly temperature independent. Instead, if the linewidth would be caused by damping, a significant temperature dependence would be expected. Therefore we conclude that the two peaks (HS and LS) most likely are a superposition of two or more individual peaks; this view is supported by the results obtained from DFT calculations (*vide infra*).

3.4 DFT calculations

Simulations of the inelastic part of the NIS spectra on the basis of DFT calculations [19] are shown in Figure 8b. The group of peaks around 50 meV for the LS state and around 30 meV for the HS state are in agreement with the experimental observation. These peaks correspond to normal modes involving only Fe-N bond stretching as for example indicated in Figure 9. The observed bond distances from DFT geometry optimizations will be compared below with results obtained by EXAFS.

Due to the almost octahedral environment of the iron center three out of six Fe-N stretching modes are invisible in NIS and IR spectra. Those modes that transform according to the A_{1g} and E_g representations of the ideal octahedron do not contribute to the msd of the iron nucleus or to the variation of the electric dipole moment. Only the remaining three modes, that transform according to the T_{1u} representations can be observed in NIS and IR spectra. These three modes, with calculated energies of 29.1, 30.1 and 35.3 meV for the HS state and 42.8, 46.6 and 52.6 meV for the LS state, give rise to prominent peaks in the simulated NIS spectra of both the LS and HS isomer of [Fe(tpa)$(NCS)_2$]. Considerable contributions to the calculated absorption probability also arise from N-Fe-N bending modes in the range from 3 to 20 meV. These modes cannot be identified in the experimental spectra because they are superimposed by modes originating from the acoustical phonons which give much larger contributions to the experimental NIS spectra.

The Fe-N bond stretching frequencies calculated for the LS isomer are about 12.4 meV smaller than the IR values given above (59.5 and 66.0 meV); however, they are in good agreement with the frequencies obtained from NIS. The broad peak at 50 meV observed in the measured NIS spectrum of the LS isomer (Fig. 8) represents the envelope of the three Fe-N stretching modes in the range of 45 to 55 meV. The pronounced peak at 30 meV in the NIS spectrum of the HS isomer is assigned to the same modes (Fig. 8). These modes reflect, according to the intensity of the peaks, the substantial contributions to the msd of the iron nucleus that is associated with the three T_{1u} Fe-N stretching modes.

According to the normal mode analysis the low-intensity peak at 66 meV in the measured NIS spectrum as well as the line at 65.7 meV in the IR spectrum must be assigned to a mode which has predominantly N-C-S bending character and to some extent Fe-N stretching character. The mixed character of this mode is due to interactions between Fe-N stretching and N-C-S bending modes, which are close in energy in the LS isomer.

The calculated N-C-S bending modes of the HS isomer do not show any admixture of Fe-N stretching modes because of the relatively large energy gap of about 30 meV between these modes. Correspondingly, the NIS spectrum of the HS isomer does not exhibit a peak at the respective energy. In summary, the measured NIS spectra of the LS isomer as well as the DFT calculations suggest, that the IR line attributed previously to an Fe-N bond stretching mode of the LS isomer [26] should be assigned to a bending mode of the NCS group instead. As a result the frequency shift of the Fe-N stretching mode upon spin crossover is about 40% smaller than assumed earlier.

In molecular crystals the Lamb-Mössbauer factor can be regarded as a product of a molecular part, $f_{\mathrm{LM}}^{\mathrm{mol}}$, and a lattice part, $f_{\mathrm{LM}}^{\mathrm{lat}}$:

$$f_{\mathrm{LM}} = f_{\mathrm{LM}}^{\mathrm{mol}}\, f_{\mathrm{LM}}^{\mathrm{lat}}. \tag{10}$$

The f_{LM} factor derived from NFS measurements comprises the molecular and the lattice part of f_{LM}. Instead,

Table 3. Factorization of the Lamb-Mössbauer factor f_{LM} into a molecular part $f_{\mathrm{LM}}^{\mathrm{mol}}$ and into a lattice part $f_{\mathrm{LM}}^{\mathrm{lat}}$ according to equation (10) at different temperatures. f_{LM} was determined by NFS, $f_{\mathrm{LM}}^{\mathrm{mol}}$ by "truncated" NIS and by DFT calculations.

T	spin	f_{LM}	$f_{\mathrm{LM}}^{\mathrm{mol}}$		$f_{\mathrm{LM}}^{\mathrm{lat}}$	
(K)	state	NFS	NIS	DFT	NIS	DFT
34	LS	0.68	0.85	0.92	0.80	0.74
107	HS	0.38	0.86	0.75	0.44	0.51
200	HS	0.20	0.80	0.52	0.25	0.38

an estimate of the molecular part $f_{\mathrm{LM}}^{\mathrm{mol}}$ only is obtained by integrating over the 'molecular part' of the NIS spectrum, *i.e.* after truncating its low-energy part (0–15 meV) which mainly accounts for the lattice contribution $f_{\mathrm{LM}}^{\mathrm{lat}}$. Jung *et al.* [3,4] pointed out that the factorization of the Lamb-Mössbauer factor is in fact more complicated, since individual molecular and lattice parts have to be considered for each vibrational mode. For the present qualitative comparison of f_{LM} contributions, however, we neglect this sophisticated approach. The f_{LM} values resulting from DFT calculations, from NFS spectra and from "truncated" NIS spectra for the HS and LS isomers of [Fe(tpa)(NCS)$_2$] are listed in Table 3. At all temperatures the total Lamb-Mössbauer factor, f_{LM}, that is retrieved from NFS, is considerably smaller than the molecular part, $f_{\mathrm{LM}}^{\mathrm{mol}}$, which is determined either by NIS or by DFT. Using equation (10) at low temperature (34 K) an estimate of 0.75 to 0.80 can be given for the lattice part of the Lamb-Mössbauer factor, $f_{\mathrm{LM}}^{\mathrm{lat}}$, depending on the method that is used for determining $f_{\mathrm{LM}}^{\mathrm{mol}}$. At higher temperatures (200 K) an almost constant $f_{\mathrm{LM}}^{\mathrm{mol}}$ results from NIS while the DFT calculations give a decrease of $f_{\mathrm{LM}}^{\mathrm{mol}}$ by almost 50% when increasing the temperature from 34 K to 200 K. This decrease is caused by the excitations of low-energy (<10 meV) molecular vibrations, which contribute to the msd of the iron nucleus. These vibrations have been neglected when $f_{\mathrm{LM}}^{\mathrm{mol}}$ was determined from the NIS spectra.

3.5 EXAFS

The extended X-ray absorption fine structure (EXAFS) signal is a direct measure of the radial distribution of the backscattering atoms around the absorbing atom. The fine structure was extracted with the computer program package EXPROG [31] and analysed with EXCURV98 [32] using the small atom approximation, a Hedin-Lundquist potential [33] for the excited state and a van Barth potential [34] for the ground state. The structural parameters were refined by minimisation of χ^2. The structural model applied in the refinement of the fine structure is defined by the symmetry of the iron site. The six nitrogen atoms were grouped together to one shell at about 2 Å, accounting for the backscattering in the EXAFS of [Fe(tpa)(NCS)$_2$] in the LS state (Fig. 10). To calculate the multiple-scattering contributions, the NCS groups and the aromatic rings of the tpa moiety were treated as separate units. Mössbauer spectroscopy has shown, that at

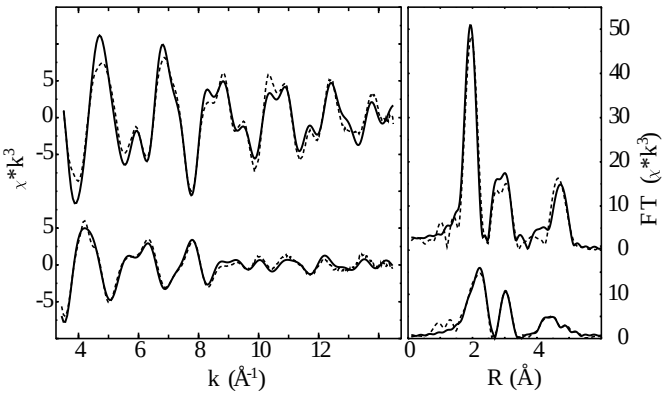

Fig. 10. EXAFS (left panel) and Fourier transform (right panel) of [Fe(tpa)(NCS)$_2$] obtained at 30 K (top) and 200 K (bottom). The dashed lines represent the measured data and the solid lines are the fit curves.

Table 4. Measured and calculated Fe-N bond lengths (Å) for the HS and LS isomers of [Fe(tpa)(NCS)$_2$].

Spin state	Method	Fe-N_{NCS}	Fe-N_{tpa}
LS	B3LYP/6-311G*	1.91	1.93
	EXAFS (30 K)	1.959(3)	1.959(3)
HS	B3LYP/6-311G*	2.08	2.23
	EXAFS (200 K)	2.066(8)	2.216(5)

30 K less than 2% of the iron is in the HS state and at about 200 K less than 2% are in the LS state. Therefore we have chosen these temperatures for the structural analysis with EXAFS. In the LS state the Fourier transform of the EXAFS spectrum is dominated by the 6 nitrogen ligands at about 2 Å (Tab. 4). Furthermore, strong contributions at 3 Å and at 4.7 Å are present (Fig. 10). The latter two are enhanced due to strong multiple scattering, which is a result of the quasi linear arrangement of the NCS ligands. The differences in distance between the nitrogen atoms in the first coordination sphere appeared to be too small to be resolved in a fit with two different nitrogen contributions in this shell for the LS isomer.

For the HS state the EXAFS amplitude is much smaller due to the higher static and thermal structural disorder and because of the destructive interference of the N_{NCS} and N_{tpa} contributions in the first shell. Again three peaks dominate the Fourier transform. One is accounting for the N_{NCS} atoms at a distance of about 2.1 Å and for the N_{tpa} atoms at a distance of about 2.2 Å from the iron, one for the C atoms at 3 Å (strongly enhanced by multiple scattering) and one for the contributions at 4.5 Å which are dominated by the sulfur atoms of the two NCS groups (also enhanced by multiple scattering). In contrast to the LS isomer, in the HS isomer the contributions of the nitrogen atoms from tpa and NCS are clearly resolved, *i.e.* for N_{NCS} at a distance of 2.066(8) Å and for N_{tpa} at 2.216(5) Å from the iron site.

4 Conclusions

Nuclear resonance scattering of synchrotron radiation has successfully been applied to a spin-crossover complex. Compared to energy-resolved MS the time-resolved NFS takes advantage of the properties of synchrotron radiation such as high brilliance and pulsed time structure. The recorded data are practically free from background originating from electronic scattering in the sample or from high energy radiation as emitted by radioactive sources. The effective thickness and from this the Lamb-Mössbauer factor can be directly measured, no corrections for saturation effects or source parameters are necessary. NIS yields information about molecular vibrations which cannot be obtained from NFS or conventional MS. Compared to other methods like inelastic neutron scattering, inelastic X-ray scattering, IR and Raman spectroscopy, NIS probes only those molecular vibrations in which the resonant iron nuclei in the compound under study is involved. Furthermore, NIS provides a precise energy reference by itself whereas for the other methods the energy has to be analysed separately.

The results on $[Fe(tpa)(NCS)_2]$ represent the first study obtained from a set of NFS measurements on a complete temperature scan over a spin-crossover transition. These data benefit in particular from the direct measurement of $t_{\rm eff}$ within a large time window for the delayed radiation. The directly and accurately measured discontinuous behaviour of $t_{\rm eff}$ by NFS in the spin-transition region confirms earlier results obtained by conventional MS on other compounds of this family. Related parameters such as $f_{\rm LM}$, Θ_D and msd of the ^{57}Fe atom reveal different behaviour for the LS and HS isomers. NIS measurements and DFT calculations together provide information about the intra-molecular part $f_{\rm LM}^{\rm mol}$ and allow to determine the vibrational modes of $[Fe(tpa)(NCS)_2]$; *i.e.* the Fe-N bond stretching vibrations of both the LS and the HS isomers could unambiguously be identified. NIS turned out to be powerful as a complementary tool for IR and Raman spectroscopy. The observed bond distances from DFT geometry optimizations are in good agreement with the corresponding results obtained by EXAFS.

The authors thank the ESRF services for support during the nuclear resonant scattering experiments. This work was finacialy supported by the German Research Foundation (DFG), the German Federal Ministery for Education, Science, Research and Technology (BMBF), the European Union (ERB-FMRX-CT-0199) *via* the TMR-TOSS-network and the European Synchrotron Radiation Facility (ESRF) in Grenoble, France.

References

1. P. Gütlich, A. Hauser, H. Spiering, Angew. Chemie **106**, 2109 (1994); Angew. Chem., Int. Ed. Engl. **33**, 2024 (1994).
2. E. König, Struct. Bonding (Berlin) **76**, 51 (1991).
3. J. Jung, H. Spiering, Z. Yu, P. Gütlich, Hyperfine Interact. **95**, 107 (1995).
4. J. Jung, Ph.D. Thesis, Johannes Gutenberg-Universität Mainz, Germany (1995).
5. J.B. Hastings, D.P. Siddons, U. van Bürck, R. Hollatz, U. Bergmann, Phys. Rev. Lett. **66**, 770 (1991).
6. G.V. Smirnov, Hyperfine Interact. **97/98**, 551 (1996).
7. E. Gerdau (ed.), Hyperfine Interact. **123/124** (1999).
8. M. Seto, Y. Yoda, S. Kikuta, X. W. Zhang, M. Ando, Phys. Rev. Lett. **74**, 3828 (1995); W. Sturhahn, T.S. Toellner, E.E. Alp, X. Zhang, M. Ando, Y. Yoda, S. Kikuta, M. Seto, C.W. Kimball, B. Dabrowski, *ibid.* **74**, 3832 (1995).
9. K.S. Singwi, A. Sjœlander, Phys. Rev. **120**, 1093 (1960).
10. R. Rüffer, A.I. Chumakov, Hyperfine Interact. **97/98**, 589 (1996).
11. H. Grünsteudel, Ph.D. Thesis, Lübeck (1998).
12. W. Sturhahn, E. Gerdau, Phys. Rev. B **49**, 9285 (1994).
13. R.F. Pettifer, C. Hermes, J. Phys. C **8**, 127 (1986).
14. O. Kahn, *Molecular Magnetism* (VCH Publishers Inc., New York, 1993).
15. A.D. Becke, J. Chem. Phys. **98**, 5648 (1993); C. Lee, W. Yang, R.G. Parr, Phys. Rev. B **37**, 785 (1988).
16. M.J. Frisch *et al.*, Gaussian 98, Revision A.7, Gaussian Inc., Pittsburgh PA (1998).
17. J.S. Binkley, J.A. Pople, W.J. Hehre, J. Am. Chem. Soc. **102**, 939 (1980); M.S. Gordon, J.S. Binkley, J.A. Pople, W.J. Pietro, W.J. Hehre, *ibid.* **104**, 2797 (1982); W.J. Pietro, M.M. Francl, W.J. Hehre, D.J. Defrees, J.A. Pople, J.S. Binkley, *ibid.* **104**, 5039 (1982); A.J.H. Wachters, J. Chem. Phys. **52**, 1033 (1970); P.J. Hay, *ibid.* **66**, 4377 (1977).
18. M.W. Wong, Chem. Phys. Lett. **256**, 391 (1996).
19. H. Paulsen, H. Winkler, A.X. Trautwein, H. Grünsteudel, V. Rusanov, H. Toftlund, Phys. Rev. B **59**, 975 (1999).
20. P. Gütlich, Struct. Bonding (Berlin) **44**, 83 (1981).
21. Z. Yu, G. Schmitt, S. Hofmann, H. Spiering Y.F. Hsia, P. Gütlich, Hyperfine Interact. **93**, 1459 (1994).
22. V. Schünemann, H. Winkler, Rep. Prog. Phys. **63**, 263 (2000).
23. H. Welker, Diplom thesis, Physikalisches Institut der Universität Erlangen (1994).
24. H.F. Grünsteudel, Diplom thesis, Physikalisches Institut der Universität Erlangen (1993).
25. D. Barb, *Grundlagen und Anwendungen der Mössbauerspektroskopie* (Akademie Verlag, Berlin, 1980).
26. F. Højland, H. Toftlund, S. Yde-Andersen, Acta Chem. Scand. A **37**, 251 (1983).
27. J.H. Takemoto, B. Hutchinson, Inorg. Chem. **12**, 705 (1973).
28. H. Grünsteudel, H. Paulsen, W. Meyer-Klaucke, H. Winkler, A.X. Trautwein, H.F. Grünsteudel, A.Q.R. Baron, A.I. Chumakov, R. Rüffer, H. Toftlund, Hyperfine Interact. **113**, 311 (1998).
29. H. Paulsen, R. Benda, C. Herta, V. Schünemann, A. I. Chumakov, L. Duelund, H. Winkler, H. Toftlund, A.X. Trautwein, Phys. Rev. Lett. **86**, 1351 (2001).
30. A. Chumakov, R. Rüffer, O. Leupold, H. Grünsteudel, A. Barla, T. Asthalter, *ESRF Highlights-1999* (ESRF, Grenoble, 2000), p. 50.
31. H.F. Nolting, C. Hermes, EMBL data analysis and evaluation program package, EMBL outstation Hamburg (1992).
32. N. Binsted, S.S. Hasnain, J. Syn. Rad. **3**, 185 (1996).
33. L. Hedin, Lundqvist, in *Solid State Physics*, Vol. 23, edited by F. Seitz, D. Turnbull, H. Ehrenreich (Academic Press, New York, 1969), p. 1
34. U.V. Barth, L. Hedin, J. Phys. C **5**, 1629 (1972).